WP17ER-PR(18) 21217

S Taimourzadeh et al.

Verification and validation of integrated simulation of e nergetic particles in fusion plasmas I: linear simulations

Preprint of Paper to be submitted for publication in
Nuclear Fusion

This work has been carried out within the framework of the EUROfusion Consortium and has received funding from the Euratom research and training programme 2014-2018 under grant agreement No 633053. The views and opinions expressed herein do not necessarily reflect those of the European Commission.

Verification and validation of integrated simulation of energetic particles in fusion plasmas I: linear simulations

S. Taimourzadeh[1], E. M. Bass[2], Y. Chen[3], C. Collins[4], N. N. Gorelenkov[5], A. Könies[6], Z. X. Lu[7,8], D. A. Spong[9], Y. Todo[10], M. E. Austin[12], J. Bao[1], M. Borchardt[6], A. Bottino[7], W. W. Heidbrink[1], Z. Lin[1], R. Kleiber[6], A. Mishchenko[7], L. Shi[1], J. Varela[9], R. E. Waltz[4], G. Yu[11], W. L. Zhang[1,13], and Y. Zhu[11]

E-mail: zhihongl@uci.edu

[1]University of California, Irvine, CA, 92697, USA

[2]University of California San Diego, San Diego, California 92093, USA

[3]University of Colorado at Boulder, Boulder, Colorado 80309, USA

[4]General Atomics, PO Box 85608, San Diego, CA 92186-5608, USA

[5]Princeton Plasma Physics Laboratory, Princeton University, Princeton, New Jersey 08543, USA

[6]Max Planck Institute for Plasma Physics, D-17491 Greifswald, Germany

[7]Max Planck Institute for Plasma Physics, 85748 Garching, Germany

[8]Fusion Simulation Center, Peking University, Beijing 100871, Peoples Republic of China

[9]Oak Ridge National Laboratory, Oak Ridge, TN 37831, USA

[10]National Institute for Fusion Science, Toki, Japan

[11]University of California, Davis, CA, 95616, USA

[12]University of Texas, Austin, TX, 78712, USA

[13]Beijing National Laboratory for Condensed Matter Physics and CAS Key Laboratory of Soft Matter Physics, Institute of Physics, Chinese Academy of Sciences, Beijing 100190, China

Abstract. This paper reports verification and validation of linear simulations of Alfv́en eigenmodes in DIII-D shot #159243 using eight gyrokinetic, gyrokinetic-MHD hybrid, and eigenvalue codes. Using classical fast ion profile, all simulation codes find that reversed shear Alfv́en eigenmodes (RSAE) is the dominant instability. The real frequencies from all codes have a coefficient of variation less than 5% for the most unstable modes with toroidal mode number $n = 4$ and 5. The simulated frequencies agree much better with the experimental frequencies at the time of 790 ms, rather than the 805 ms at which time the equilibrium is used in the simulations. The simulated growth rates exhibit greater variations and pressure gradients of thermal plasmas make significant contribution to the growth rates. Mode structures of the dominant modes agree well among all codes. Using the outward-shifted fast ion profile calculated from a reduced transport model, toroidal Alfv́en eigenmode (TAE) with $n = 6$ is found to be unstable in the outer edge, consistent with the experimental data. Variations of the real frequencies and growth rates of the TAE are slightly larger than those of the RSAE. Finally, Electron temperature fluctuations and radial phase shifts from

simulations show no significant differences with the experimental data for the strong $n = 4$ RSAE, but significant differences for the weak $n = 6$ TAE.

1. Introduction

Energetic particle (EP) confinement is a key physics issue for the burning plasma experiment ITER, since ignition relies on self-heating by energetic fusion products (α-particles). EP transport can affect plasma profiles, beam deposition, and current drive, and can erode reactor walls [1]. Due to the strong coupling of EP with burning thermal plasmas, plasma confinement properties in the ignition regime are some of the most uncertain factors when extrapolating from existing tokamaks to the ITER. Fully self-consistent simulation of EP transport and EP coupling with thermal plasmas must incorporate magnetohydrodynamic (MHD) processes with kinetic effects of both EP and thermal plasmas on an equal footing, which requires an integrated kinetic-MHD simulation model based on the gyrokinetic formalism [2]. Coordinated efforts in verification and validation (V&V) are needed to develop the integrated simulation for EP transport due to mesoscale Alfv́enic instabilities primarily excited by EP and EP coupling with microturbulences and macroscopic MHD modes mostly driven by thermal plasmas.

Initial V&V studies of the linear gyrokinetic simulations of reversed shear Alfv́en eigenmodes (RSAE) excited by fast ions from neutral beam injection (NBI) in the advanced tokamak regime of the DIII-D experiment have been carried out [3] by using a gyrokinetic particle code GTC [4], a gyrokinetic continuum code GYRO [5], and a gyro-Landau fluid code TAEFL [6]. Good agreements in RSAE frequency, growth rate, and mode structure have been obtained among these initial value simulations, and between simulation results and experimental measurements using electron cyclotron emission imaging (ECEI) [7]. The successful linear V&V lend some degree of confidence to nonlinear gyrokinetic simulations [8]–[10] that provide new kinetic insights on nonlinear Alfv́en eigenmode dynamics and EP transport, and help the construction of reduced EP transport models [11]–[13] which are needed for fast parameter scans, shot-to-shot analysis, and optimization of ITER experiments.

The first-principles simulations and reduced transport models are built upon a hierarchical construction of EP transport prediction based on more fundamental constituents by the progression from linear dispersion relation to nonlinear dynamics and eventually to EP transport. Nonlinear V&V will take on an increased importance as gyrokinetic and kinetic-MHD hybrid simulation models progress from linear to nonlinear simulations for understanding EP confinement properties regarding instability saturation mechanisms, interactions between mesoscale EP turbulence with microturbulence and MHD modes, and EP transport statistics. While it is unlikely

that different models will agree in all situations, the regimes of deviation will need to at least be characterized and understood. This is a continuous process since models and computational methods evolve in time. As updated results become available from the first-principles models, they will provide new calibration points for the reduced EP transport models and stimulate their further development.

The V&V studies should use a hierarchical approach, starting with test cases from existing experiments and quantities that are well-diagnosed. For this purpose, an NBI-heated low-confinement (L-mode) plasma (DIII-D discharge #159243) with many small-amplitude RSAE and TAE (toroidal Alfv́en eigenmode), significant flattening of the EP profile, and strong microturbulence [14], [15] has been selected as the reference case for V&V studies by the Integrated Simulation of Energetic Particle (ISEP) project, part of the Scientific Discovery through Advanced Computing (SciDAC) initiative. High quality data for the AE structure, frequency, and amplitude as well as the EP distribution, phase-space flows, and intermittent losses are all available from comprehensive DIII-D diagnostics. Taking advantages of these recent experimental progress, the early linear V&V studies [3] have been extended to nonlinear V&V studies of EP transport by using more newly available EP simulation codes and new EP reduced transport models. Linear and nonlinear simulations of AE and microturbulence in this reference case have been carried out by gyrokinetic, kinetic-MHD hybrid, and eigenvalue codes. Modeling of EP transport have also been carried out by reduced transport models. These V&V studies will proceed from linear simulation of instabilities, to nonlinear simulation of saturation mechanisms, to coupling of mesoscale turbulence with microturbulence and MHD modes, and finally to reduced EP transport models. This paper reports the linear simulations as the first step in these V&V studies.

In this paper, we present linear simulations of RSAE and TAE observed in shot #159243 by using five initial value gyrokinetic codes (EUTERPE [16], GEM [17], GTC, GYRO, ORB5 [18]), two initial value kinetic-MHD codes (FAR3D [19], MEGA [20]), and a perturbative eigenvalue code (NOVA-K [21]). Since fast ion profiles have the biggest uncertainty among all equilibrium profiles measured in the experiment, we use the fast ion profiles both from the kinetic EFIT reconstruction [22] accounting only collisional transport, and from the more realistic the kick model [13] taking into account EP transport by RSAE and TAE. Using the EFIT fast ion profile, all simulation codes find that RSAE is the dominant instability. The real frequencies from all eight codes have a coefficient of variation (CV) less than 5% for the most unstable modes with toroidal mode number $n = 4$ and 5. The simulated frequencies agree much better with the ECE frequencies at the experimental time of 790 ms, rather than the 805 ms at which time the equilibrium is used in the simulations. This is probably due to limitations in the accuracy of the safety factor q_{min} calculated in the EFIT reconstruction. The simulated growth rates of these two RSAE exhibit greater variations with a CV up to 17% for the five gyrokinetic codes, and a CV up to 26% for all eight codes. Mode structures of the dominant modes agree well among all seven non-perturbative codes regarding radial eigenmodes, 2D shape on poloidal plane, ballooning characteristics,

radial extent, and radial symmetry breaking. The TAE observed in the outer edge of the DIII-D experiment is not found in these initial value simulations using the EFIT fast ion profile, indicating that TAE is either linearly stable or sub-dominant to the RSAE. Using the outward-shifted fast ion profile from the kick model, GTC simulations find the $n = 6$ TAE to be the dominant instability in the outer edge, consistent with the ECE data. Variations of the real frequencies and growth rates from seven simulation codes are slightly larger than those of the RSAE, partially due to the co-existence of multiple radial eigenmodes with similar frequencies and growth rates. Finally, GTC simulation data have been processed by the Synthetic Diagnostic Platform (SDP) [23] to produce electron temperature fluctuations and radial phase shifts, which show no significant differences for the strong $n = 4$ RSAE, but significant differences for the weak $n = 6$ TAE. These linear results provide a necessary foundation for the next step of nonlinear V&V studies.

The rest of the paper is organized as follows. In Sec. 2, we describe the RASE and TAE observations in the DIII-D experiment, and the equilibrium and profiles of this experiment as used in all simulation codes. In Sec. 3, we compare different physics models and numerical parameters used in this V&V by all simulation codes. In Sec. 4, we quantify the agreements and differences in RSAE and TAE linear dispersion from these eight independently developed simulation codes. In Sec. 5, we process GTC data by a synthetic diagnostics to compare simulation results with the experimental ECE and ECEI data. Conclusions and discussions are presented in Sec. 6.

2. DIII-D EP Experiment for Verification and Validation

This work uses profiles and magnetic equilibrium obtained from DIII-D shot 159243 during L-mode at 805 ms, which has a safety factor q profile with reversed shear and 6.4 MW of early beam power injected at 70-81 keV to excite multiple unstable RSAEs and TAEs. This discharge has excellent diagnostic coverage and was examined extensively in studies [14], [15], [24] of AE-induced fast-ion transport in critical gradient experiments. Figure 1(a) shows the spectrogram of electron cyclotron emission (ECE) data during the current ramp for shot #159243, along with calculated RSAE frequency evolution from an ad hoc model [25]. The model was used to constrain the value of q_{min} for the kinetic EFIT equilibrium reconstruction used in section 2.1. As described in [24], a more realistic fast-ion pressure profile was obtained using the time-dependent kick model of AE transport [26], where AE mode structures were scaled to experiment measurements at a single timeslice and then evolved in time (figure 1(b)) so that the modeled neutron rate matched the measured value. The resulting fast-ion profile agrees well with experimental measurements [15]. The kick model fast ion pressure profile is used in section 4.2.

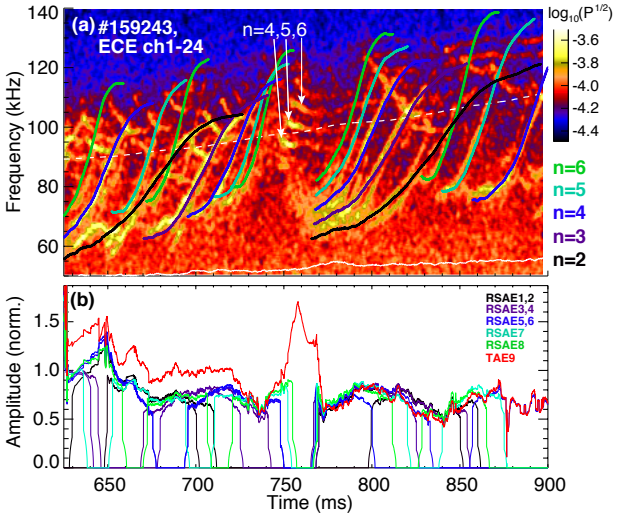

Figure 1. Adapted from [24]. (a) ECE power spectrum with RSAE time evolution fits from an ad hoc model [25]. (b) Time evolution of amplitudes determined from the kick model for DIII-D shot #159243.

2.1. Equilibrium and profile comparison

All benchmarking codes use magnetic equilibrium calculated from EFIT [27], except for FAR3D and EUTERPE which use the same equilibrium calculated from VMEC [28]. Profiles are obtained using kinetic EFIT calculations. Figure 2 shows the equilibrium and profiles for all codes, as outputted from each code, after the experimental inputs have been internally processed. Figures 2(a) depicts 10 magnetic flux surfaces ranging from $\rho = 0.1 - 1.0$ in uniform steps, where ρ is the square root of the toroidal flux normalized by its separatrix value. Figure 2(b) shows the magnetic field magnitude on the low and high field sides of the mid-plane, respectively. Magnetic surfaces align within tolerance and magnetic field magnitudes are almost identical with the exception that it, on the low field side at $\rho = 1.0$, is 3% larger in NOVA. Figures 2(c - d) show that the q profile, density profiles, and temperature profiles are almost identical for all codes.

3. Simulation Models

This paper presents linear AE simulations of the DIII-D EP experiment described in Sec. 2 by using a perturbative eigenvalue code (NOVA-K), and seven non-perturbative initial value codes including five gyrokinetic codes (EUTERPE, GEM, GTC, GYRO, ORB5) and two gyrokinetic-MHD hybrid codes (FAR3D, MEGA). A tabulated comparison of the different codes is presented in table 1.

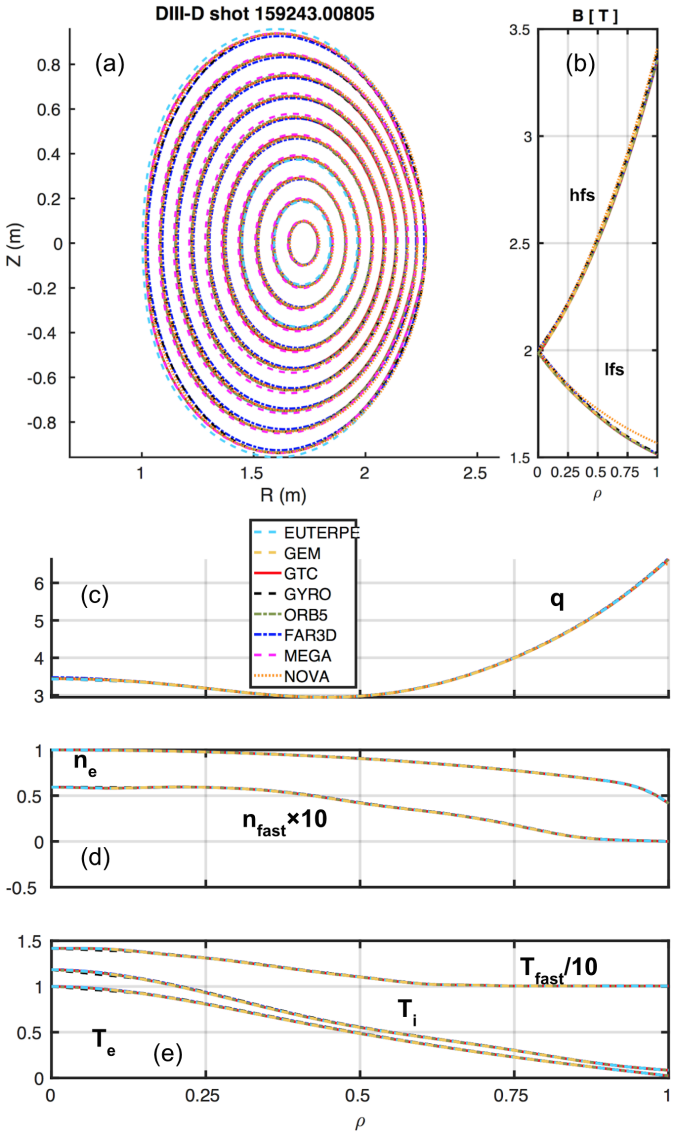

Figure 2. Equilibrium geometry and profiles, for DIII-D shot 158243 at 805 ms, outputted from all benchmarking codes, after experimental inputs have been processed. (a) 10 magnetic flux surfaces ranging from $\rho = 0.1 - 1.0$. (b) Magnetic field amplitude on the mid-plane for the high field side and low field side. (c) q profile. (d) Electron and fast ion densities normalized to the electron on axis value ($n_0 = 3.29 \times 10^{13} cm^{-3}$). (e) Electron, thermal ion, and fast ion temperatures normalized to the electron on axis value ($T_{e,0} = 1689eV$).

3.1. Gyrokinetic model

3.1.1. EUTERPE EUTERPE is three dimensional, full volume, and electromagnetic gyrokinetic particle in cell (PIC) code. It solves the gyrokinetic Vlasov-Maxwell system neglecting $\tilde{B}_{||}$ perturbations. To avoid numerical difficulties associated with the so-called "cancellation problem", the gyrokinetic equations are formulated using mixed variables [29] and the "pullback transformation scheme" [16]. It can be interpreted as an explicit reset of the time integrator bringing the system back to the $v_{||}$ scheme [30].

The spatial directions are discretized with B-splines (here B-splines of order two have been used). The code uses Fourier filtering of the perturbations in the angular directions. Furthermore, the sparse matrices resulting from the finite element decomposition have been Fourier transformed and filtered to construct a Fourier solver guaranteeing high accuracy. The spatial resolution is provided by using 150 radial and 128 poloidal splines. It is possible to provide a leading Fourier factor ($\sim e^{i(m_p\theta+n_p\phi)}$), which is called "phase factor" in code terminology. It allows to single out the toroidal direction [31] and allows a lower resolution in poloidal direction.

The Vlasov equation is solved using the so-called δf-ansatz [32], i.e. the distribution function is split into an equilibrium part and the perturbation. The number of marker particles is 64 million for the ions, 256 million for the electrons and 64 million for the fast ions.

The equilibrium provided by a mapping from the computational domain extends from $r = 0$ to $r = a$ with Dirichlet boundary conditions at the outer boundary and natural boundary conditions for the radial finite elements at the inner. Lost particles are re-inserted such that their weight is zero and the constants of motion are preserved.

Although there are several models of different physical complexities installed in the EUTERPE code, such as fluid electrons and/or ions (FLU-EUTERPE) [33] or perturbative kinetic MHD model (CKA-EUTERPE) [34], here always the full gyrokinetic model with a realistic electron/ion mass ratio is used.

The electrons are drift kinetic i.e. their gyro-radius is zero, while for the ion species the gyro-averages resulting from the theory are performed with n_g-point averages where n_g ranges between 4 and 32 and adapts to the size of the gyro-radii [35].

3.1.2. GEM GEM is a gyrokinetic delta-f PIC code that was originally developed for the study of tokamak core plasma microturbulence and anomalous transport. GEM uses the field-aligned coordinates in general magnetic equilibria. Electromagnetic perturbations are included using the parallel canonical momentum formalism. The split-weight scheme [17], [36] is used to enhance the time step otherwise limited by the fast electron motion along the magnetic field. GEM also has a fluid electron model for studying the long wavelength energetic particle-driven modes [37]. The fluid electron model consists of the electron continuity equation, the isothermal condition for the electron temperature and the Ohm's law for determining the parallel electric field. The fluid electron model is used for this paper. The simulation domain is $0.1 < r/a < 0.9$, with a grid resolution of $(N_x, N_y, N_\parallel) = (256, 64, 64)$ in the field-line-following coordinates (x, y, z), with 16 particles/cell per ion species.

3.1.3. GTC The gyrokinetic code (GTC) [4], [38] is a full torus particle code using both the δf and full-f methods. Thermal and fast ions are simulated using gyrokinetic equation [39]. Electron drift kinetic equation can be solved either exactly using a conservative scheme for both tearing and non-tearing parity [40], or approximately using a fluid-kinetic hybrid electron model that removes the tearing parity [41]. The

perturbed electromagnetic field is solved from the gyrokinetic Poisson's equation [42] and Ampère's Law. GTC has been widely used to study microturbulence [43], Alfven eigenmodes [44], and other low frequency MHD modes in the tokamaks, stellarators [45], and field-reversed configuration [46].

For the present work, marker particles are loaded in velocity space according to a Maxwellian distribution, f_0, and the plasma perturbation is described via the δf method. The electrons are modeled according to the fluid-kinetic hybrid model [41], [47]. In the lowest order, or adiabatic limit, electrons are described via the fluid continuity equation. In the higher orders, kinetic effects are solved by the particle method for the non-adiabatic part of the electrons distribution using the drift kinetic equation. In this study, we neglect $\delta B_{\|}$ effects [48]. The simulation domain used is $\rho = [0.12, 0.9]$, the time step size is $\Delta t = 0.14 R_0/v_{A0}$, where v_{A0} and R_0 are the on axis Alfvén speed and major radius, $\Delta r/\rho_i \sim r\Delta\theta/\rho_i \sim 1.7$, where Δr and $r\Delta\theta$ are the radial and poloidal grid spacing, and ρ_i is the local thermal ion gyro-radius. Each particle species has 20 particles per cell.

3.1.4. GYRO GYRO [5], [49] is a continuum gyrokinetic code with field-aligned coordinates in kinetic phase space: flux-surface label $\hat{r} = \frac{r}{a}$, where r is the flux-surface half width at the centroid height and a is the plasma minor radius; normalized parallel orbit time τ; pitch angle variable $\lambda = \frac{v_\perp^2}{v^2 \hat{B}}$, where $v_\perp$ and v are the perpendicular and total velocities and $\hat{B}$ is the magnetic field normalized to a reference value; and kinetic energy K normalized to the local temperature T: $\hat{E} = \frac{K}{T}$. The toroidal degree of freedom is treated spectrally. Trapped and passing particles lie on separate phase-space grid points, with τ normalized as is appropriate. The gyrokinetic equations are solved for three kinetic species: electrons, thermal deuterium ions, and hot beam deuterium ions modeled with an equivalent high temperature Maxwellian distribution. Coupling between species occurs through a Poisson-Ampere field solve performed at each time step. The solver considers electrostatic potential ϕ and perpendicular magnetic field fluctuations (through perturbed parallel vector potential $A_{||}$), but neglects parallel magnetic field fluctuations. Both ion species are treated gyrokinetically and the electrons are treated with drift kinetics. The Eulerian timestep uses a hybrid implicit-explicit scheme, with the electron dynamics treated implicitly to avoid tracking stiff electron parallel motion.

The present linear simulations are performed over a radial domain $r = [0.23, 0.83]$ or $\rho = [0.20, 0.81]$, with a grid resolution $(N_{\hat{r}}, N_\tau, N_\lambda, N_{\hat{E}}) = (150, 20, 8, 8)$ at each value of toroidal mode number n. The λ grid includes 4 passing and 4 trapped values. Radial grid points are nonuniformly spaced to optimize resolution of flux surfaces. This gives a mean radial grid spacing of nearly two thermal ion Larmor radii, inadequate for resolving ion-scale drift-wave turbulence but well converged for the presented EP-driven Alfvn eigenmodes. The required time step of $\frac{c_s \Delta t}{a} = 0.01$ is smaller than typical values used for simulating microturbulence due to the faster EP dynamics.

3.1.5. ORB5 ORB5 is a nonlinear gyrokinetic PIC code [18] with extension to electromagnetic physics and multiple species [50]–[52]. The $p_{\|}$ formulation is used and the adjustable control variate method is implemented in ORB5 [50], [53], in order to avoid the "cancellation problem". Recent development in ORB5 allows larger time step size due to the implementation of the "pullback transformation scheme" [16], [29]. The linear, quadratic and cubic splines are implemented in the code for discretization in radial and poloidal directions and the cubic spline is used in this work. The Fourier representation is used in the toroidal direction. Fourier filters are applied in poloidal and toroidal directions in addition to a field-aligned filter which keeps the poloidal harmonics in the range $nq - \Delta m \leq m \leq nq + \Delta m$ and in this work, $\Delta m = 5$ for RSAE simulation and $\Delta m = 16$ for TAE simulation.

The simulation is performed in radial domain $\rho = [0, 1.0]$, with a grid resolution of $(N_\rho, N_\theta, N_\phi) = (256, 192, 48)$ for RSAE simulation, where θ and ϕ are poloidal-like and toroidal angles. The number of marker particles is 16 million thermal ions, 64 million for electrons and 16 million fast ions for $n = 4, 5$ RSAEs. Doubled marker numbers are adopted for $n = 3, 6$ RSAEs. Gyro-averages are included for all species and the points number for gyro-average is determined by using the gyro-adaptive method [54]. The time step size is $0.065 R_0/v_{A0}$, where v_{A0} and R_0 are the on axis Alfvén velocity and major radius. While the traditional δf method and the direct δf method [55] are both implemented in the code, the former one is adopted in the simulation.

3.2. Gyrokinetic-MHD hybrid

3.2.1. MEGA MEGA is a hybrid simulation code for energetic particles interacting with an MHD fluid [20], [56]–[58]. The large fast ion pressure profile flattening and the electron temperature fluctuations due to the TAEs observed in a DIII-D experiment were successfully reproduced by comprehensive MEGA simulations [58]. In the MEGA code, the bulk plasma is described by the nonlinear MHD equations, and the energetic particles are simulated with the gyrokinetic PIC method. The electromagnetic field is given by the MHD model. The effects of the energetic particles on the MHD fluid is taken into account through the perpendicular energetic particle current in the MHD momentum equation. Either the full f method or the δf method can be applied to the energetic particles. The thermal ion diamagnetic drift is considered in the MHD momentum equation, and the finite Larmor radius effect is retained for the energetic particle dynamics. The spatial derivatives in the MHD equations are calculated with a fourth order finite difference method, and the fourth order Runge-Kutta scheme is employed for the time integration of both the MHD equations and the particle dynamics. For the benchmark results presented in this paper, $(128, 16, 256)$ grids are used for cylindrical coordinates (R, φ, z), respectively, with $0 \leq \varphi < \pi/2$ for the study of the n=4 RSAE.The number of computational particles is 1 million.

3.2.2. FAR3D Gyro-Landau closure techniques [59] allow excitation of Alfv́en instabilities within a hybrid (fluid-kinetic) global model; this technique was originally implemented and applied in the TAEFL model [6], [60], and more recently extended to 3D configurations with the FAR3D model [19], [61]. The motivations for such models are: computational efficiency; the fact that the equations can be cast into a matrix eigenmode form, allowing examination of both growing/damped modes, and the capability to follow long-time scale nonlinear phenomena [62]. For the calculations reported here, the FAR3D model was used; this model is based on VMEC equilibria and can treat both 2D and 3D configurations as well as up-down asymmetric tokamaks. The initial equilibrium is obtained from EFIT; this is converted to a VMEC input file and then recalculated using VMEC. The VMEC data is transformed to Boozer coordinates [63], which are the native coordinates used in the code. The version of FAR3D used for this study included two moment equations (density and parallel momentum) for the fast ion component; options are available with three and four moments, which allow extension of the model [64] to non-Maxwellian distribution functions, such as slowing-down distributions. The fast ion moment equations include four scalar closure coefficients [63] that are selected via calibration against analytical results for Alfv́en instability growth rates. The MHD component of the FAR3D model is based on the reduced MHD approximation; a poloidal flux evolution equation (Ohms law), a toroidal component of the vorticity equation, and a pressure and parallel velocity evolution equation for the thermal plasma (to include sound wave couplings) are included. Toroidal rotation is included, but not used for this paper. Finite Larmor radius effects are introduced into the fast ion equations using Padé approximate fits to the Bessel functions and for the thermal ions using a perturbative approach. Ion and electron Landau damping is included through perturbative terms in the vorticity equation [65]. Since separate equations for thermal electrons and ions are not currently implemented, an ω^* ion correction is added to the real frequencies of the modes analyzed in this paper. The equations are solved using Fourier series representations for the poloidal and tororidal angle dependencies; the radial variable is the square-root of the normalized toroidal magnetic flux and a finite difference grid is used in this coordinate. The equations can either be integrated in time, using a semi-implicit stepping procedure, or as a single eigenmode solution, based on a targeted Jacobi-Davidson algorithm. For the calculations reported in this paper 400 radial surfaces were used, with 22 to 30 Fourier modes for the perturbed fields and 10 Fourier modes for the equilibrium fields. In most of the cases in this paper, the eigensolver option was used instead of the initial value option, since the instabilities studied here had growth rates that were subdominant to other AE and MHD modes.

3.3. Perturbative eigenvalue NOVA simulations

NOVA and NOVA-K codes are linear hybrid MHD/kinetic codes to study EP driven MHD eigenmode instabilities. NOVA solves ideal MHD equations and finds eigenmodes, such as TAEs [21], including such effects as plasma compressibility and realistic

geometry. NOVA-K evaluates the wave particle interaction of the eigenmodes of interest such as TAEs or RSAEs by employing the quadratic form with the perturbed distribution function of energetic ions coming from the drift kinetic equations [66]. NOVA-K is able to predict various kinetic growth and damping rates perturbatively, such as the phase space gradient drive from energetic particles, continuum damping, radiative damping, ion/electron Landau damping and trapped electron collisional damping. NOVA is routinely used for AE structure computations and comparisons with the experimentally observed instabilities [7], [67]. The main limitations of NOVA code are caused by neglecting thermal ion FLR, toroidal rotation, and drift effects in the eigenmode computations. Therefore it can not describe accurately radiative damping for example. Finite element methods are used in radial direction and Fourier harmonics are used in poloidal and toroidal directions. In the results reported here we used the uniform in ψ radial grid with 201 and 256 points in radial and poloidal directions respectively, and poloidal harmonics ranging from 7 to 32.

Table 1. Comparison of simulation models used in this benchmark.

code	electrons	ions	fast ions	$\delta B_{\parallel}$	type
EUTERPE	PIC DK	PIC GK	PIC GK	no	initial value
GEM	fluid	PIC GK	PIC GK	no	initial value
GTC	fluid-kinetic hybrid	PIC GK	PIC GK	no	initial value
GYRO	continuum DK	continuum GK	continuum GK	no	initial value
ORB5	PIC DK	PIC GK	PIC GK	no	initial value
FAR3D	fluid+perturbative landau damping	fluid+perturbative landau damping	gyrofluid closures	no	initial value
MEGA	fluid	fluid	PIC GK	yes	initial value
NOVA	fluid	fluid	kinetic	yes	eigenvalue

4. Simulation Results

4.1. RSAE

Using the equilibrium and profiles from figure 2, linear electromagnetic simulations from all codes find an unstable RSAE, peaked at the $q_{min} = 2.94$ surface, to be the dominant linear instability for DIII-D shot #159243 at 805 ms. The RSAE linear dispersion has been obtained and is presented in figure 3. In the figure, codes are grouped according to physics model via the plot marker used. Namely, diamond, star, and circle markers are used for the gyrokinetic, gyrokinetic-MHD hybrid, and perturbative eigenvalue codes, respectively.

All models show excellent agreement in real frequency. The coefficients of variation of real frequency values, $CV_\omega = \sigma_\omega/\mu_\omega$, where σ and μ are the standard deviation and mean, respectively, for all data points per toroidal mode number in the dispersion are presented in table 2. $CV_\omega < 5\%$ throughout the dispersion, with the exception of the subdominant toroidal mode, $n = 3$, where $CV_\omega = 8.40\%$. Figure 3 also contains ECE

measured frequency values, which are shifted into the plasma frame, and are grouped with square plot markers. The ECE values are plotted for two experimental times in the discharge, 790 ms and 805 ms, to give a qualitative estimation of rate of change of the experimental q_{min} value. Simulation results agree better with the ECE frequency value at 790 ms, which is due to limitations in the accuracy of the q_{min} calculation in the equilibrium reconstruction. For context, errors as small as 1% in q_{min} can lead to variations in frequency as high as 18%. q_{min} can be manually changed until simulation frequency values agree with the ECE data at 805 ms,but here we accept the EFIT calculations as they are.

Growth rates exhibit greater variations than those in the real frequency comparison. Nonetheless, there is agreement in the general trend of the dispersion, with $n = 4$ or 5 being the dominant mode. FAR3D and NOVA show exceptions to this trend, as the growth rates are found to increase monotonically. For NOVA, this is expected as some damping mechanisms are ignored, such as the radiative damping for RSAEs which is expected to increase strongly with the toroidal mode number. For TAE modes the radiative damping is added via the analytic expression developed earlier [68]. The $n = 6$ data for GYRO is not presented here, as a coexistent ITG mode was observed to affect the numerical properties of the simulation. The coefficient of variation for $n = 4$, 5 is $CV_\gamma = 16.3\%$, 17.1%, for the gyrokinetic codes, and $CV_\gamma = 17.8\%$, 26.1% for all codes.

Table 2. Real Frequency Coefficients of Variation

	n=3	n=4	n=5	n=6
CV_ω	8.42%	4.78%	4.02%	4.76%

Even with physics model differences, mode structures agree well between all codes. Figure 4 shows the radial structures of the poloidally-rms-averaged dominant poloidal harmonic, and two accompanying side bands, for the $n = 4$ RSAE. All codes show maximum mode intensity localized near the q_{min} surface, $\rho = 0.44$, with the FWHM coefficient of variation of the dominant poloidal harmonic being $CV_{FWHM} = 7.7\%$, and 14.5% for the gyrokinetic codes and all of the codes, respectively. Figure 5 shows the two dimensional RSAE eigenfunction structures, which show agreement in 2D shape on the poloidal plane, ballooning characteristics, radial extent and radial symmetry breaking. In the MHD limit the Alfvén mode structure is up-down symmetric; the presence of an EP component breaks this symmetry and leads to the teardrop/triangular shaped mode structures. These drift effects on TAE mode structures were first presented in Figure 14 of Ref. [6] and later discussed for RSAE modes in Refs. [3], [64], [69].

Furthermore, the significance of the effects of thermal ion and electron gradients on the RSAE instability drive has been examined by several codes, which found that there is a large thermal plasma contribution to the destabilization of the AEs in this case, consistent with theoretical expectations [70].

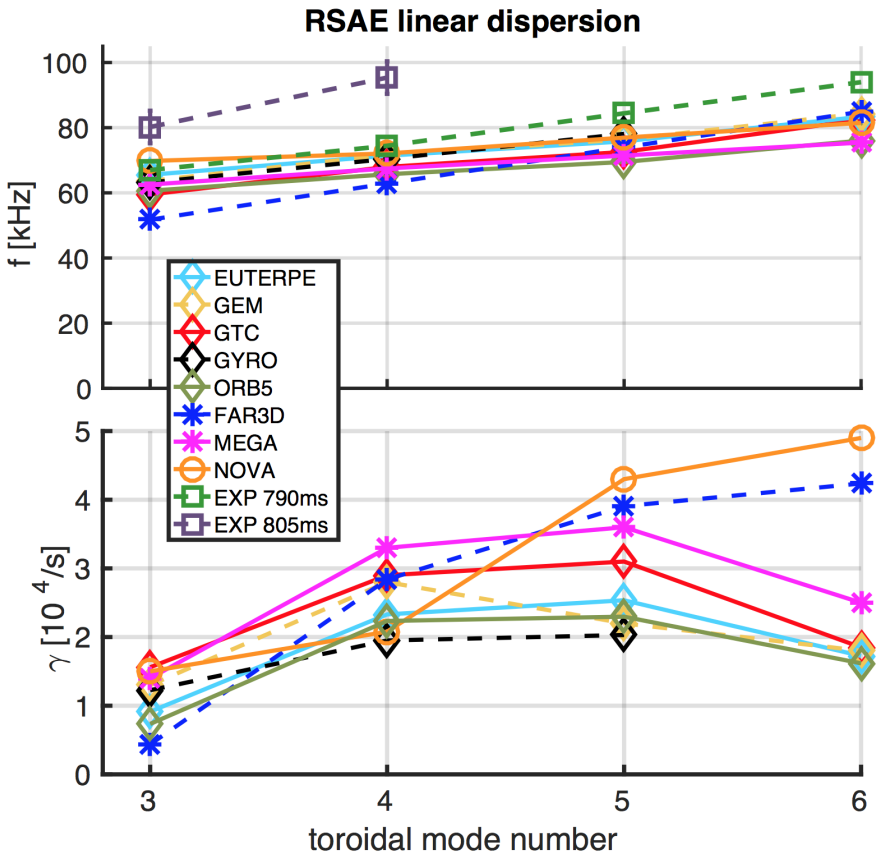

Figure 3. Linear dispersion relation calculation for RSAE in DIII-D shot 158243 at 805 ms. (a) Real frequencies. (b) Growth rates. The plot markers are diamond, star, and circle for the gyrokinetic, kinetic-MHD hybrid, and perturbative eigenvalue codes, respectively.

4.2. TAE

In addition to RSAEs, experimental observations also find unstable TAEs, as shown in figure 1. Spatial analysis of the ECE data shows that the TAEs are localized near $\rho \approx 0.75$. To see if simulation can find an unstable TAE, the radial domain is restricted to the range $\rho = [0.564 - 0.902]$ in a GTC simulation to avoid the dominant RSAE. In doing so, linear simulations do show a marginally unstable TAE with $\omega = 99$ kHz and $\gamma/\omega = 0.0121$.

To see if a linearly unstable TAE appears without artificial domain restrictions, we use a more realistic fast-ion density profile taking into account transport caused by the AE, calculated from the kick model [26]. Figure 6 compares the fast-ion density profiles from the kinetic EFIT and the kick model. The figure shows that the kick model calculation predicts a higher density and larger gradients beyond $\rho = 0.4$ than the kinetic EFIT prediction. These two profiles are used in GTC $n = 4$ and $n = 6$ simulations, using all other equilibrium quantities as shown in figure 2. Figure 7 shows the obtained 2D modes strucutres of the perturbed electrostatic potential for these four simulations. The top row shows the $n = 4$ and 6 mode structures, both of which show

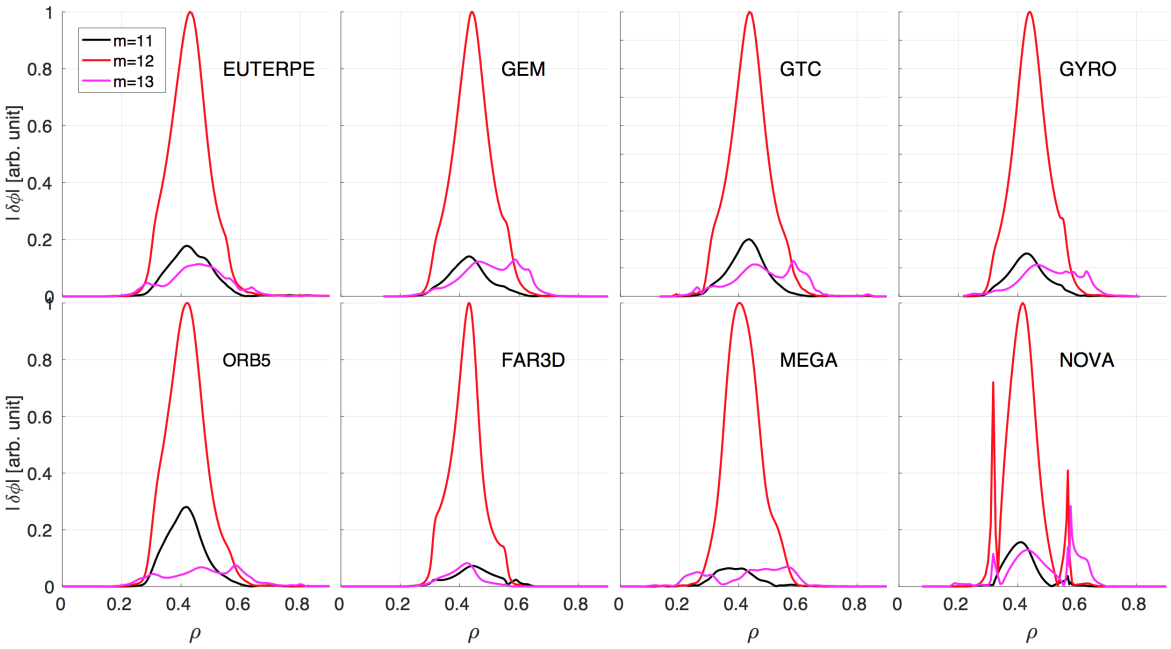

Figure 4. Poloidally-rms-averaged radial mode structures of the $n = 4$ RSAE's dominant poloidal harmonic and two side bands.

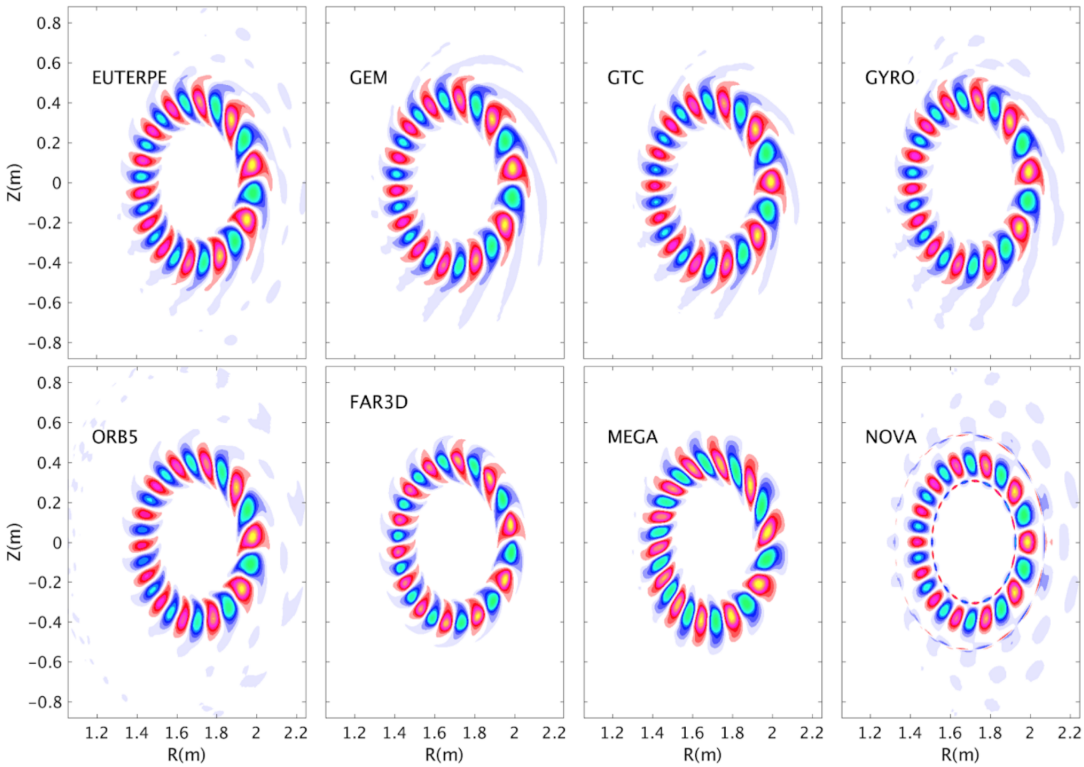

Figure 5. $n = 4$ poloidal cross section RSAE structures for DIII-D shot 158243 at 805 ms. The axes units are in meters.

an unstable RSAE, with no TAE, obtained using the kinetic EFIT profile. The bottom

row shows a transition of the dominant mode from RSAE to TAE as the toroidal mode number increases from $n = 4$ to $n = 6$. From figure 7(c), it can be seen that the dominant $n = 4$ RSAE is accompanied by a lower amplitude TAE at larger radius. The real frequency for the $n = 4$ RSAE shows almost no difference if using the kinetic EFIT or kick model profiles, but the growth rate is 30% lower when using the kick model profile.

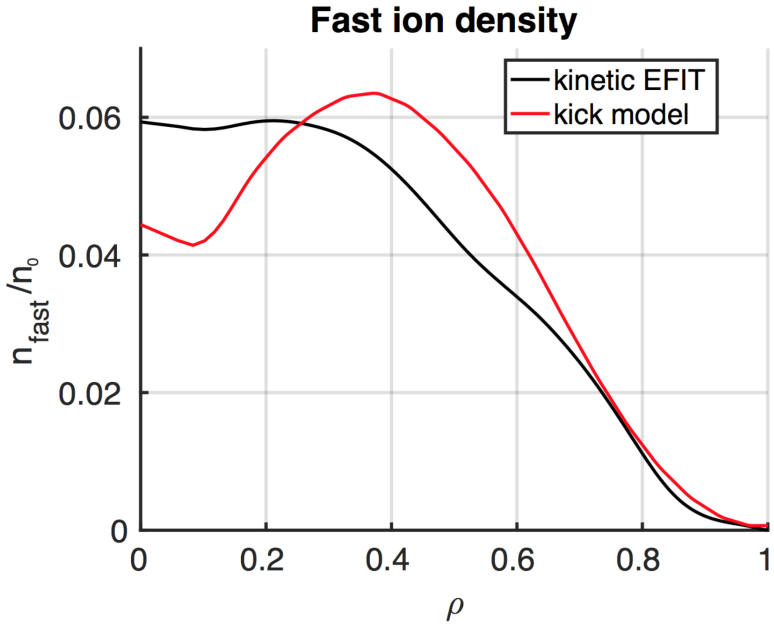

Figure 6. DIII-D shot 159243.00805 fast ion density calculation comparison of kinetic EFIT versus the kick model. $n_0 = 3.29 \times 10^{13} cm^{-3}$

After observing the differences in the fast ion density profiles between the kinetic EFIT and kick model in GTC AE simulations, a verification test is carried out for the $n = 6$ TAE mode, using the kick model fast ion density profile scaled upwards by a factor of 1.5 times. This increase of the fast-ion density is done so as to ensure that all codes yield unstable results. Table 3 tabulates the calculated TAE frequency and growth rates for $n = 6$, from seven codes, along with the measured ECE frequency (shifted into the plasma frame). The mean of the calculated real frequencies shows a 6.0% difference from the experimental ECE value, and variation between codes is characterized by $CV_\omega = 7.91\%$. Growth rates vary much more significantly, however, with $CV_\gamma = 33.1\%$ for the gyrokinetic codes. This discrepancy correlates with different observed mode structures between codes. Figure 8 shows the 2D mode structures for the perturbed electrostatic potentials in poloidal cross sections. Here, it can be seen that there are three patterns of structures, each with one, two, or three local peaks of mode amplitude. The radial eigenfunctions can be seen in figure 9, which shows the corresponding three radial eigenstates with zero, one, and two crossings of the zero value for the electrostatic potential.

The discrepancy between the mode structures between codes is consistent with

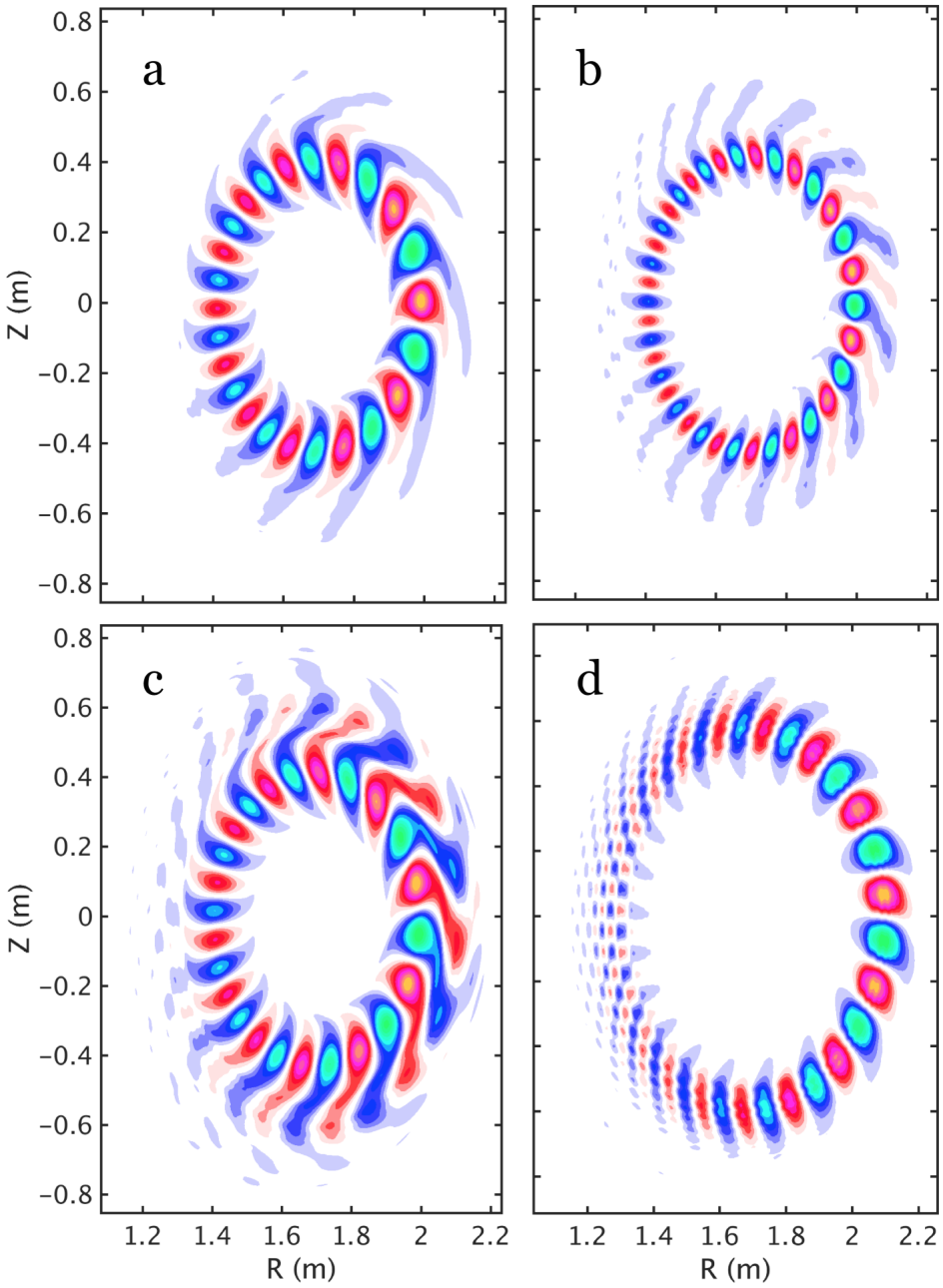

Figure 7. Perturbed electrostatic potential from GTC simulations of DIII-D shot 159243.00805. (a-b) $n = 4$ and $n = 6$ simulations, respectively, using a fast ion density profile calculated from kinetic EFIT. (c-d) $n = 4$ and $n = 6$ simulations, respectively, using a fast ion density profile calculated from the kick model.

the discrepancy in the real frequency. This is seen in a frequency scan using NOVA simulations, FAR3D's eigenvalue solver and MHD runs using the EUTERPE code. The scans reproduce the three mode structures of figure 9, and the radial structures of these three radial eigenstates are shown in Figure 10. The top row shows the NOVA scan of frequency values $f = [84.4\,92.6,\ 99.8]$ kHz, the middle row shows FAR3D scan with $f = [86.0,\ 97.7,\ 118]$ kHz and the bottom row shows the EUTERPE results with

Table 3. $n = 6$ real frequencies (in the plasma frame) and growth rates for DIII-D 159293.00805 simulations using a fast-ion density profile calculated using the kick model, scaled upwards by a factor of 1.5 times, and the corresponding coefficient of variation of the results. ECE frequency data at 805 ms is also included.

	EUTERPE	GEM	GTC	GYRO	ORB5	FAR3D	NOVA	CV_ω	ECE (805 ms)
$f\,[kHz]$	100	102	95.2	79.2	95.2	97.7	92.6	7.85%	98.9
$\gamma\,[10^3/s]$	54.4	20.7	55.8	48.3	60.7	3.56	5.35		

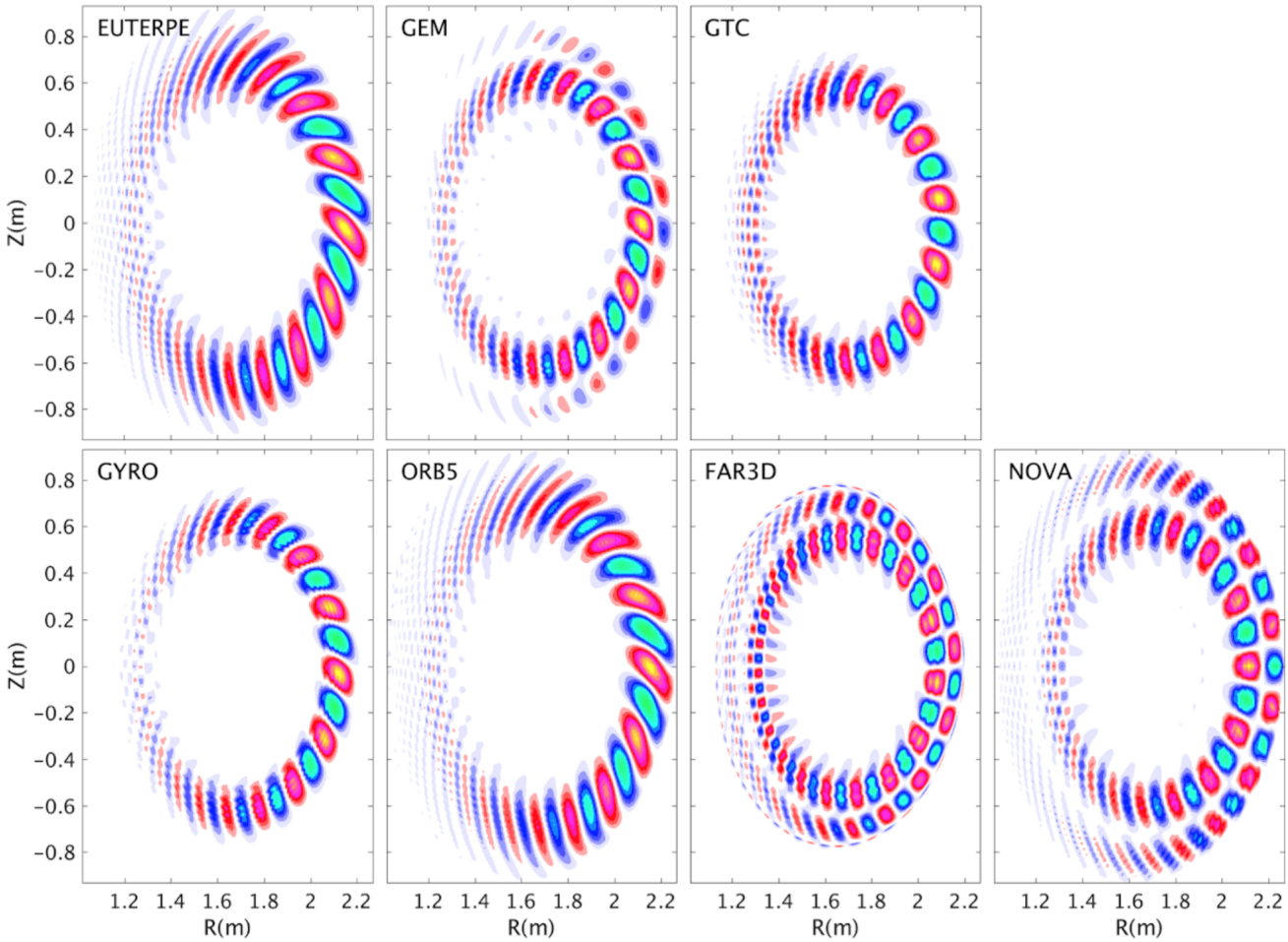

Figure 8. Poloidal cross section of the perturbed electric potential for the $n = 6$ TAE, using the kick model fast ion density profile, for DIII-D shot 158243 at 805 ms.

$f = [80.6, 88.7, 102]$ kHz.

5. Comparison to experimental values

Experimental data from the DIII-D ECE radiometer [71] has been obtained for validation purposes. The data corresponds to the lowest radial harmonic of the $n = 4$ mode, which is averaged over 11 steps in the time range [791.5, 802.5] ms of the DIII-D shot #158243. Corresponding data for the $n = 6$ mode is also obtained.

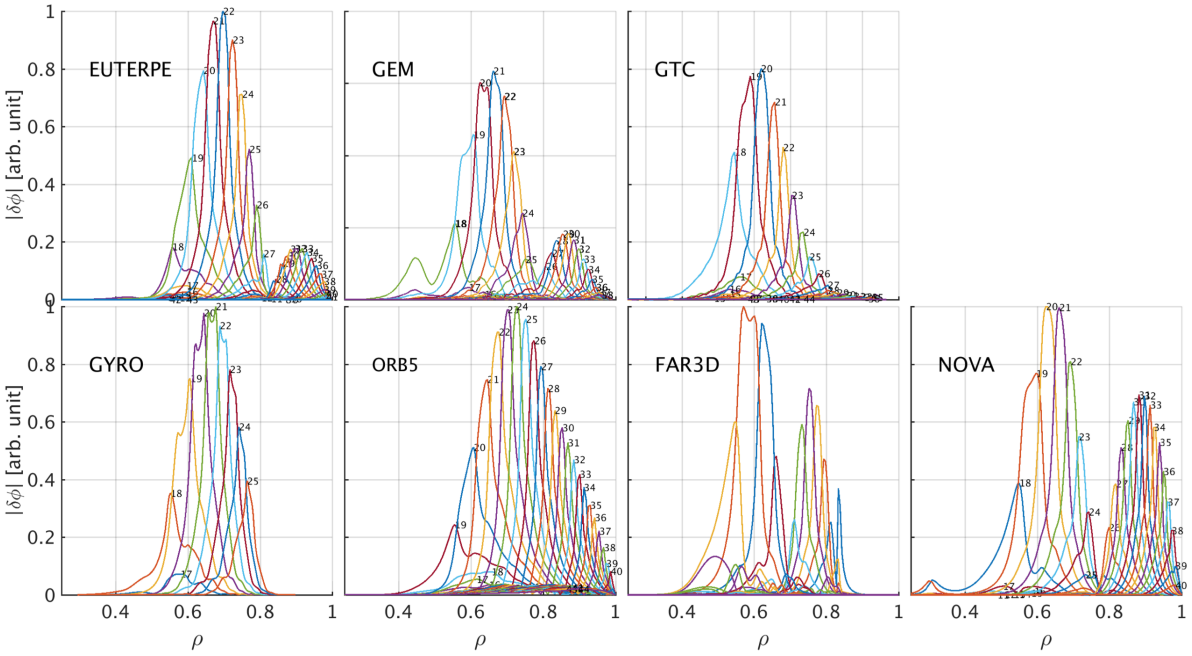

Figure 9. Radial structures of the poloidal harmonics of the electrostatic potential for the $n = 6$ TAE, using the kick model fast ion density profile, for DIII-D shot 158243 at 805 ms.

The diagnostic spans the frequency range [83.5, 129.5] GHz in 40 channels, providing diagnostic coverage in the radial range R = [148.1, 228.7] cm, where R is the major radius, 4 cm above the midplane. We compare the measured and simulated radial structure of the magnitude of the mode amplitude, $|\delta T_e|/T_{e0}$, where δT_e and T_{e0} are the perturbed and equilibrium electron temperatures, respectively, and phase profile relative to a specified radial location.

For this comparison, GTC has been interfaced with the open source Synthetic Diagnostic Platform (SDP) [23], where GTC simulation data is processed through SDP. Figure 11(a) shows $|\delta T_e|/T_{e0}$, obtained from GTC via SDP, for both the kinetic EFIT (black) and kick model (magenta) fast-ion density profiles and the experimental data (red). The GTC data corresponds to the two $n = 4$ RSAE-dominated cases in figure 7 (a) & (c). All three structures show peak amplitude near $R \approx 198$ cm. The full width half max are nearly the same, with that from the kick-model being slightly larger. These results show there is no significant difference in $|\delta T_e|/T_{e0}$ of the RSAE between simulations and the experimental data, when using either the kinetic EFIT or kick model fast ion density profiles. The experimental data may indicate the presence of radially increasing fluctuations between R = [210, 220] cm, which may correspond to TAE activity; however, the uncertainty in the data is large in that region. Figure 11(b) shows the mode's phase difference for different radial locations, relative to $R = 195.0$ cm, for the experimental data and the GTC simulations with the kinetic EFIT and kick model fast ion density profiles. The disagreement between the phase values for the GTC simulations with the kinetic EFIT and kick model fast ion density profiles in the

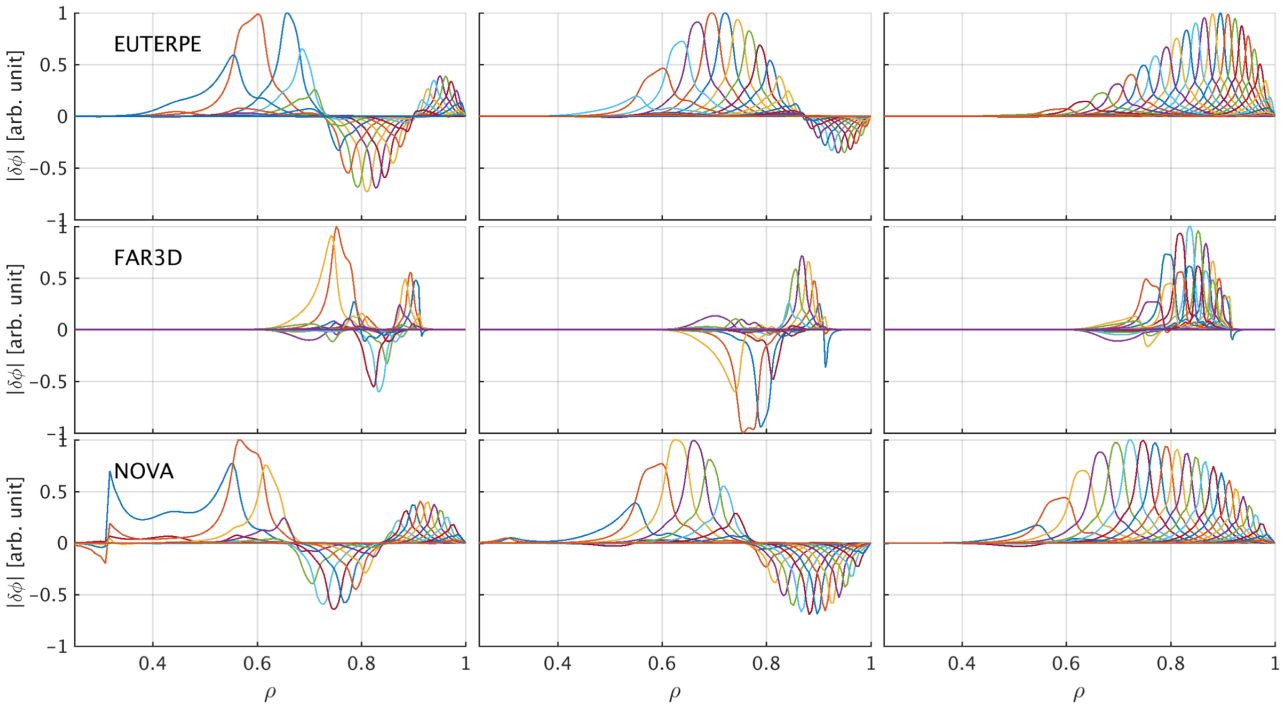

Figure 10. Radial TAE mode structures from TAE frequency scan using fast ion density calculated from the kick-model. (Top row) MHD runs using the EUTERPE code with $f = [80.6, 88.7, 102]$ kHz. (middle row) FAR3D eigenvalue runs with $f = [86.0, 97.7, 118]$ kHz. (bottom row) NOVA frequency scan with $f = [84.4, 92.6, 99.8]$ kHz. In the figure, frequencies increase from left to right.

outer radial regions is due to the presence of a subdominant TAE near $R \approx 215$ cm in the simulation using the kick model fast ion density.

Comparison of GTC $n = 6$ simulation data, via SDP, with experimental ECE data does show a significant difference between experimental data and GTC simulations using the kinetic EFIT or kick model fast-ion density calculations. Figure 12(a) shows the $|\delta T_e|/T_{e0}$ profiles for GTC simulation results and the experimental ECE data. The ECE data shows peak magnitude near $R \approx 226$ cm, and the peak amplitudes from GTC simulations are $R = 201.1$ cm and $R = 210.0$ cm for the kinetic EFIT and kick model results, respectively. Qualitatively, there is a better agreement of experimental data with the kick model result than the kinetic EFIT simulation result. The large discrepancy in location of the peak magnitude between the kick model simulation result and experiment may be attributed to the kick model's prediction of the outward shift of the fast ion density profile gradients being too modest, but further testing is needed to confirm this. Another reason for the discrepancy may be that the experimentally observed TAE is simply nonlinearly generated, which cannot be reproduced in linear simulations. Figure 12(b) shows the mode's phase difference for different radial locations, relative to $R = 221.4$ cm, for the GTC results and the experiment, in the radial range $R = [195.0, 225.0]$ cm.

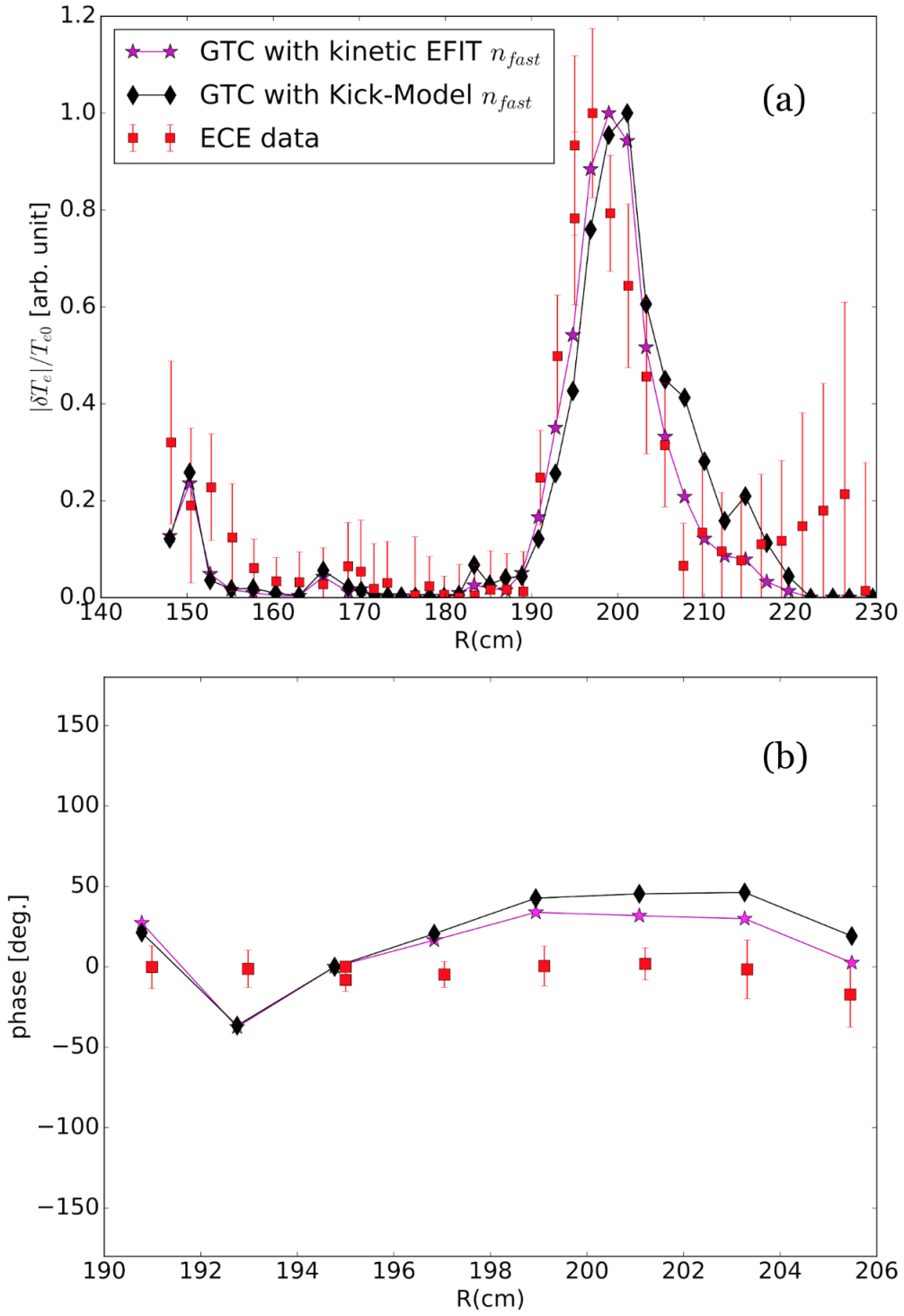

Figure 11. Comparison of GTC simulation data, after being processed through the Synthetic-Diagnostic-Platform, to experimental ECE data for DIII-D #159243 at 805 ms. (a) Radial structure of $|\delta T_e|/T_{e0}$. (b) The phase profile relative to $R = 195.0$ cm.

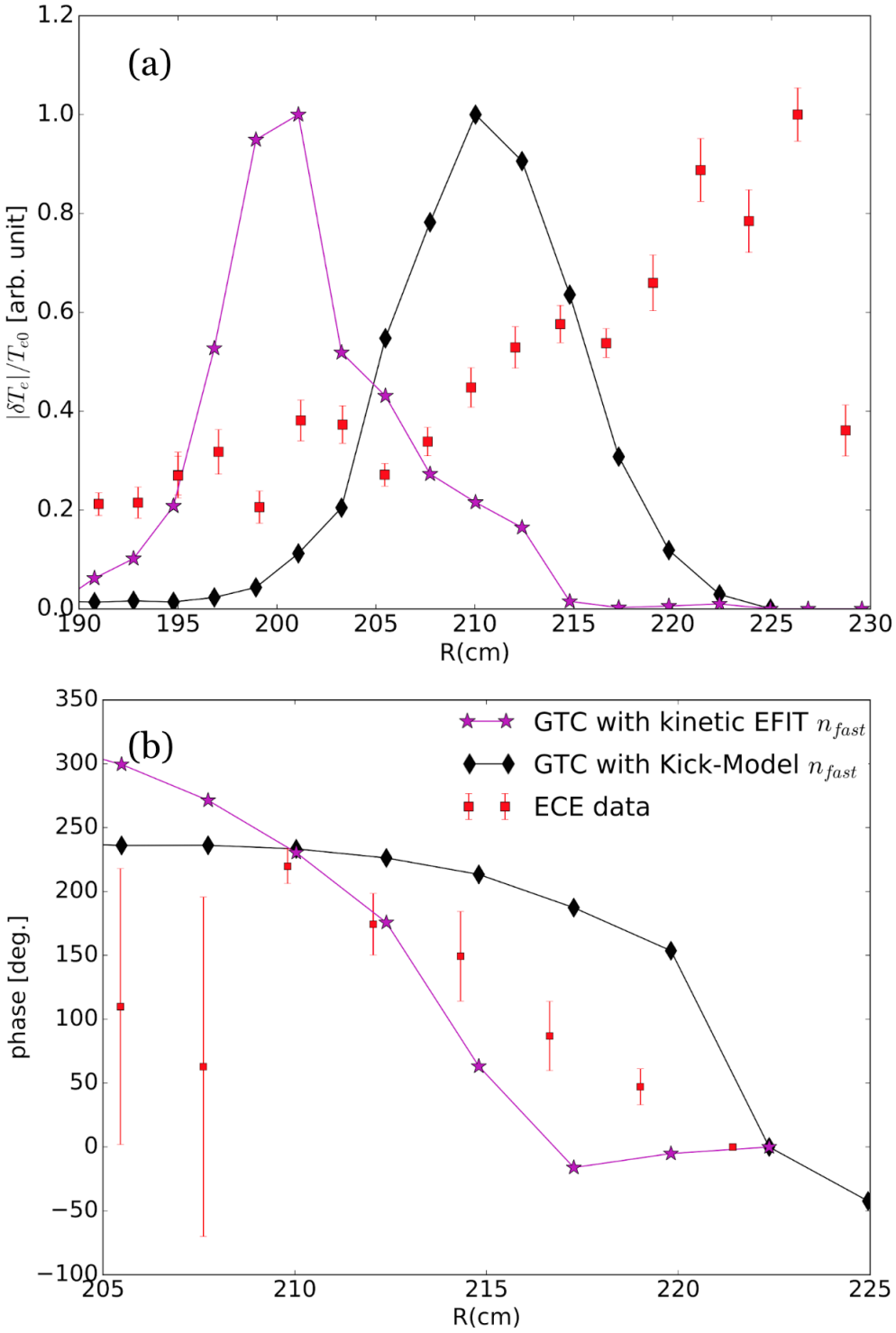

Figure 12. Comparison of GTC simulation data, after being processed through the Synthetic-Diagnostic-Platform, to experimental ECE data for DIII-D #159243 at 805 ms. (a) Radial structure of $|\delta T_e|/T_{e0}$. (b) The phase profile relative to $R = 221.4$ cm. The measured $n = 6$ TAE ECE frequency is 98.9 kHz (plasma frame) and the GTC calculated value is 95.2 kHz.

6. Conclusion and Discussion

Using kinetic EFIT equilibrium data from DIII-D shot #159243, gyrokinetic, gyrokinetic-MHD hybrid, and perturbative eigenvalue simulations have obtained the RSAE linear dispersion of toroidal mode numbers $n = [3, 6]$, for verification and validation purposes. The simulations are conducted using five initial value gyrokinetic codes (EUTERPE, GEM, GTC, GYRO, ORB5), two initial value kinetic-MHD codes (FAR3D , MEGA), and a perturbative eigenvalue code (NOVA-K). All simulation results predict a linearly unstable RSAE and find excellent agreement in mode structure and real frequency. Simulated RSAE frequencies agree well with experimental ECE values for the experimental time of 790 ms. This discrepancy is due to small error in the reconstructed equilibrium q_{min} value. Growth rates are found to show larger variance, with a coefficient of variation of 18% for the dominant mode number.

Moreover, experimental measurements observe the presence of TAE modes in the time of interest. Therefore linear simulations are repeated with a more realistic fast ion density profile obtained using the kick model, which takes AE induced transport into account. Using this fast ion profile, GTC simulations show that the observed instability transitions from RSAE to TAE as the toroidal mode number is increased from $n = 4$ to $n = 6$, whereas no TAE is observed when using the EFIT fast ion profile. TAE simulations from seven codes find variations of the real frequencies and growth rates are slightly larger than those of the RSAE, partially due to the co-existence of multiple radial eigenmodes with similar frequencies and growth rates.

Further validations are obtained by comparing GTC simulation data, processed through the Synthetic-Diagnostic-Platform, for $n = 4$ and $n = 6$, using both the kinetic EFIT and kick model predicted fast ion density profiles, to experimental ECE measurements of $|\delta T_e|/T_{e0}$ and phase profiles. The comparisons shows excellent agreement in radial the radial mode structure of $n = 4$ $|\delta T_e|/T_{e0}$, for both fast ion density profiles. The $n = 6$ comparison shows better agreement with experimental data when using the kick model fast ion density profile.

The linear RSAE V&V study presented here shows good agreement with experimental data. Nevertheless, robust comparisons of theory and experiment would require nonlinear integrated kinetic-MHD simulations, which can investigate the effects of mesoscale Alfv́enic instabilities on EP transport as well as other physical effects which cannot be captured by linear simulations. To this end, nonlinear verification studies are needed to converge theoretical calculations, and build a reliable computational toolbox to understand EP transport and aid optimizations of ITER experiments.

7. Acknowledgements

This work is supported by U.S. Department of Energy (DOE) SciDAC project ISEP, and by DOE grants DE-FG02-07ER54916 and DE-SC0013804 at UCI, DE-AC02-09CH11466 at PPPL, [ADD ADDITIONAL GRANTS/AWARDS HERE]. This work has been

carried out within the framework of the EUROfusion Consortium and has received funding from the Euratom research and training programme 2014-2018 under grant agreement No 633053. The views and opinions expressed herein do not necessarily reflect those of the European Commission. This material is based upon work using the DIII-D National Fusion Facility, a DOE Office of Science user facility, under Awards DE-FC02-04ER54698. DIII-D data shown in this paper can be obtained in digital format by following the links at [NEED GA WEBSITE LINK TO DATA HERE].

References

[1] D. C. Pace, W. W. Heidbrink, and M. A. Van Zeeland, "Keeping fusion plasmas hot," *Physics Today*, vol. 68, no. 10, 2015.

[2] L. Chen and F. Zonca, "Physics of alfvén waves and energetic particles in burning plasmas," *Reviews of Modern Physics*, vol. 88, no. 1, p. 015 008, 2016.

[3] D. A. Spong, E. Bass, W. Deng, W. Heidbrink, Z. Lin, B. Tobias, M. Van Zeeland, M. Austin, C. Domier, and N. Luhmann Jr, "Verification and validation of linear gyrokinetic simulation of alfven eigenmodes in the diii-d tokamak," *Physics of Plasmas*, vol. 19, no. 8, p. 082 511, 2012.

[4] Z. Lin, T. S. Hahm, W. Lee, W. M. Tang, and R. B. White, "Turbulent transport reduction by zonal flows: massively parallel simulations," *Science*, vol. 281, no. 5384, pp. 1835–1837, 1998.

[5] J. Candy and R. Waltz, "An eulerian gyrokinetic-maxwell solver," *Journal of Computational Physics*, vol. 186, no. 2, pp. 545–581, 2003.

[6] D. Spong, B. Carreras, and C. Hedrick, "Linearized gyrofluid model of the alpha-destabilized toroidal alfvén eigenmode with continuum damping effects," *Physics of Fluids B: Plasma Physics*, vol. 4, no. 10, pp. 3316–3328, 1992.

[7] M. A. Van Zeeland, G. J. Kramer, M. E. Austin, R. L. Boivin, W. W. Heidbrin, M. A. Makowski, G. R. McKee, R. Nazikian, W. M. Solomon, and G. Wang, "Radial structure of Alfvén eigenmodes in the diii-d tokamak through electron-cyclotron-emission measurements," *Phys. Rev. Letters*, vol. 97, Sep. 2006.

[8] E. Bass and R. Waltz, "Gyrokinetic simulations of mesoscale energetic particle-driven alfvénic turbulent transport embedded in microturbulence," *Physics of Plasmas*, vol. 17, no. 11, p. 112 319, 2010.

[9] H. Zhang, Z. Lin, I. Holod, *et al.*, "Nonlinear frequency oscillation of alfvén eigenmodes in fusion plasmas," *Physical review letters*, vol. 109, no. 2, p. 025 001, 2012.

[10] Y. Chen, T. Munsat, S. Parker, W. Heidbrink, M. Van Zeeland, B. Tobias, and C. Domier, "Gyrokinetic simulations of reverse shear alfvén eigenmodes in diii-d plasmas," *Physics of Plasmas*, vol. 20, no. 1, p. 012 109, 2013.

[11] E. M. Bass and R. Waltz, "Nonlinear verification of a linear critical gradient model for energetic particle transport by alfvén eigenmodes," *Physics of Plasmas*, vol. 24, no. 12, p. 122 302, 2017.

[12] N. N. Gorelenkov, V. N. Duarte, M. Podesta, and H. L. Berk, "Resonance line broadened quasi-linear (rbq) model for fast ion distribution relaxation due to alfvénic eigenmodes," *Nuclear Fusion*, 2018.

[13] M. Podestà, M. Gorelenkova, N. Gorelenkov, and R. White, "Computation of alfvèn eigenmode stability and saturation through a reduced fast ion transport model in the transp tokamak transport code," *Plasma Physics and Controlled Fusion*, vol. 59, no. 9, p. 095 008, 2017.

[14] C. Collins, W. Heidbrink, M. Austin, G. Kramer, D. Pace, C. Petty, L. Stagner, M. Van Zeeland, R. White, Y. Zhu, *et al.*, "Observation of critical-gradient behavior in alfvén-eigenmode-induced fast-ion transport," *Physical review letters*, vol. 116, no. 9, p. 095 001, 2016.

[15] W. Heidbrink, C. Collins, M. Podestà, G. Kramer, D. Pace, C. Petty, L. Stagner, M. Van Zeeland, R. White, and Y. Zhu, "Fast-ion transport by alfvén eigenmodes above a critical gradient threshold," *Phys. Plasmas*, vol. 24, p. 056 109, 2017.

[16] A. Mishchenko, A. Könies, R. Kleiber, and M. Cole, "Pullback transformation in gyrokinetic electromagnetic simulations," *Physics of Plasmas*, vol. 21, no. 9, p. 092 110, 2014.

[17] Y. Chen and S. E. Parker, "A δf particle method for gyrokinetic simulations with kinetic electrons and electromagnetic perturbations," *Journal of Computational Physics*, vol. 189, no. 2, pp. 463–475, 2003.

[18] S. Jolliet, A. Bottino, P. Angelino, R. Hatzky, T.-M. Tran, B. McMillan, O. Sauter, K. Appert, Y. Idomura, and L. Villard, "A global collisionless pic code in magnetic coordinates," *Computer Physics Communications*, vol. 177, no. 5, pp. 409–425, 2007.

[19] J. Varela, D. Spong, and L. Garcia, "Analysis of alfvén eigenmode destabilization by energetic particles in large helical device using a landau-closure model," *Nuclear Fusion*, vol. 57, no. 4, p. 046 018, 2017.

[20] Y. Todo and T. Sato, "Linear and nonlinear particle-magnetohydrodynamic simulations of the toroidal alfvén eigenmode," *Physics of Plasmas*, vol. 5, no. 5, pp. 1321–1327, 1998. DOI: 10.1063/1.872791.

[21] C. Z. Cheng and M. S. Chance, "Low-n shear Alfvén spectra in axisymmetric toroidal plasmas," *Phys. Fluids*, vol. 29, pp. 3695–3701, Nov. 1986.

[22] L. Lao, J. Ferron, R. Groebner, W. Howl, H. S. John, E. Strait, and T. Taylor, "Equilibrium analysis of current profiles in tokamaks," *Nuclear Fusion*, vol. 30, no. 6, p. 1035, 1990.

[23] L. Shi, E. Valeo, B. Tobias, G. Kramer, L. Hausammann, W. Tang, and M. Chen, "Synthetic diagnostics platform for fusion plasmas," *Review of Scientific Instruments*, vol. 87, no. 11, p. 11D303, 2016.

[24] C. Collins, W. Heidbrink, M. Podestà, R. White, G. Kramer, D. Pace, C. Petty, L. Stagner, M. Van Zeeland, Y. Zhu, *et al.*, "Phase-space dependent critical gradient behavior of fast-ion transport due to alfvén eigenmodes," *Nuclear Fusion*, vol. 57, no. 8, p. 086 005, 2017.

[25] M. Van Zeeland, W. Heidbrink, S. Sharapov, D. Spong, A. Cappa, X. Chen, C. Collins, M. García-Muñoz, N. Gorelenkov, G. Kramer, *et al.*, "Electron cyclotron heating can drastically alter reversed shear alfvén eigenmode activity in diii-d through finite pressure effects," *Nuclear Fusion*, vol. 56, no. 11, p. 112 007, 2016.

[26] M. Podesta, M. Gorelenkova, and R. White, "A reduced fast ion transport model for the tokamak transport code transp," *Plasma Physics and Controlled Fusion*, vol. 56, no. 5, p. 055 003, 2014.

[27] L. Lao, H. S. John, R. Stambaugh, A. Kellman, and W. Pfeiffer, "Reconstruction of current profile parameters and plasma shapes in tokamaks," *Nuclear fusion*, vol. 25, no. 11, p. 1611, 1985.

[28] S. P. Hirshman and J. Whitson, "Steepest-descent moment method for three-dimensional magnetohydrodynamic equilibria," *The Physics of fluids*, vol. 26, no. 12, pp. 3553–3568, 1983.

[29] A. Mishchenko, M. Cole, R. Kleiber, and A. Könies, "New variables for gyrokinetic electromagnetic simulations," *Physics of Plasmas*, vol. 21, no. 5, p. 052 113, 2014. DOI: 10.1063/1.4880560.

[30] R. Kleiber, R. Hatzky, A. Könies, A. Mishchenko, and E. Sonnendrücker, "An explicit large time step particle-in-cell scheme for nonlinear gyrokinetic simulations in the electromagnetic regime," *Physics of Plasmas*, vol. 23, no. 3, p. 032 501, 2016. DOI: 10.1063/1.4942788.

[31] M. Fivaz, S. Brunner, G. de Ridder, O. Sauter, T. Tran, J. Vaclavik, L. Villard, and K. Appert, "Finite element approach to global gyrokinetic particle-in-cell simulations using magnetic coordinates," *Computer Physics Communications*, vol. 111, no. 1, pp. 27–47, 1998, ISSN: 0010-4655. DOI: https://doi.org/10.1016/S0010-4655(98)00023-X. [Online]. Available: http://www.sciencedirect.com/science/article/pii/S001046559800023X.

[32] A. Y. Aydemir, "A unified monte carlo interpretation of particle simulations and applications to non neutral plasmas," *Physics of Plasmas*, vol. 1, no. 4, pp. 822–831, 1994. DOI: 10.1063/1.870740.

[33] M. Cole, A. Mishchenko, A. Könies, R. Kleiber, and M. Borchardt, "Fluid electron, gyrokinetic ion simulations of linear internal kink and energetic particle modes," *Physics of Plasmas*, vol. 21, no. 7, p. 072 123, 2014. DOI: 10.1063/1.4890833.

[34] T. B. Fehér, "Simulation of the interaction between alfvén waves and fast particles," PhD thesis, Universität Greifswald, 2013.

[35] R. Hatzky, T. M. Tran, A. Könies, R. Kleiber, and S. J. Allfrey, "Energy conservation in a nonlinear gyrokinetic particle-in-cell code for ion-temperature-gradient-driven modes in θ-pinch geometry," *Physics of Plasmas*, vol. 9, no. 3, pp. 898–912, 2002. DOI: 10.1063/1.1449889.

[36] W. Lee, J. Lewandowski, T. Hahm, and Z. Lin, "Shear-alfven waves in gyrokinetic plasmas," *Physics of Plasmas*, vol. 8, no. 10, pp. 4435–4440, 2001.

[37] Y. Chen and S. Parker, "A gyrokinetic ion zero electron inertia fluid electron model for turbulence simulations," *Physics of Plasmas*, vol. 8, no. 2, pp. 441–446, 2001.

[38] Y. Xiao, I. Holod, Z. Wang, Z. Lin, and T. Zhang, "Gyrokinetic particle simulation of microturbulence for general magnetic geometry and experimental profiles," *Physics of Plasmas*, vol. 22, no. 2, p. 022 516, 2015.

[39] A. Brizard and T. Hahm, "Foundations of nonlinear gyrokinetic theory," *Reviews of modern physics*, vol. 79, no. 2, p. 421, 2007.

[40] J. Bao, Z. Lin, and Z. Lu, "A conservative scheme for electromagnetic simulation of magnetized plasmas with kinetic electrons," *Physics of Plasmas*, vol. 25, no. 2, p. 022 515, 2018.

[41] W. Deng, Z. Lin, and I. Holod, "Gyrokinetic simulation model for kinetic magnetohydrodynamic processes in magnetized plasmas," *Nuclear Fusion*, vol. 52, no. 2, p. 023 005, 2012.

[42] W. Lee, "Gyrokinetic particle simulation model," *Journal of Computational Physics*, vol. 72, no. 1, pp. 243–269, 1987.

[43] H. Xie, Y. Xiao, and Z. Lin, "New paradigm for turbulent transport across a steep gradient in toroidal plasmas," *Physical review letters*, vol. 118, no. 9, p. 095 001, 2017.

[44] Y. Liu, Z. Lin, H. Zhang, and W. Zhang, "Excitation of low frequency alfven eigenmodes in toroidal plasmas," *Nuclear Fusion*, vol. 57, no. 11, p. 114 001, 2017.

[45] D. A. Spong, I. Holod, Y. Todo, and M. Osakabe, "Global linear gyrokinetic simulation of energetic particle-driven instabilities in the lhd stellarator," *Nuclear Fusion*, vol. 57, no. 8, p. 086 018, 2017.

[46] L. Schmitz, D. Fulton, E. Ruskov, C. Lau, B. Deng, T. Tajima, M. Binderbauer, I. Holod, Z. Lin, H. Gota, *et al.*, "Suppressed ion-scale turbulence in a hot high-β plasma," *Nature communications*, vol. 7, p. 13 860, 2016.

[47] I. Holod, W. Zhang, Y. Xiao, and Z. Lin, "Electromagnetic formulation of global gyrokinetic particle simulation in toroidal geometry," *Physics of Plasmas*, vol. 16, no. 12, p. 122 307, 2009.

[48] G. Dong, J. Bao, A. Bhattacharjee, A. Brizard, Z. Lin, and P. Porazik, "Gyrokinetic particle simulations of the effects of compressional magnetic perturbations on drift-alfvenic instabilities in tokamaks," *Physics of Plasmas*, vol. 24, no. 8, p. 081 205, 2017.

[49] J. Candy and R. E. Waltz, "Anomalous transport scaling in the diii-d tokamak matched by supercomputer simulation," *Phys. Rev. Lett.*, vol. 91, p. 045 001, 4 Jul. 2003. DOI: 10.1103/PhysRevLett.91.045001. [Online]. Available: https://link.aps.org/doi/10.1103/PhysRevLett.91.045001.

[50] A. Bottino, T. Vernay, B. Scott, S. Brunner, R. Hatzky, S. Jolliet, B. McMillan, T.-M. Tran, and L. Villard, "Global simulations of tokamak microturbulence: finite-β effects and collisions," *Plasma Physics and Controlled Fusion*, vol. 53, no. 12, p. 124 027, 2011.

[51] A. Bottino and E. Sonnendrücker, "Monte carlo particle-in-cell methods for the simulation of the vlasov–maxwell gyrokinetic equations," *Journal of Plasma Physics*, vol. 81, no. 5, 2015.

[52] A. Biancalani, A. Bottino, M. Cole, C. Di Troia, P. Lauber, A. Mishchenko, B. Scott, and F. Zonca, "Nonlinear interplay of alfvén instabilities and energetic particles in tokamaks," *Plasma Physics and Controlled Fusion*, vol. 59, no. 5, p. 054 004, 2017.

[53] R. Hatzky, A. Könies, and A. Mishchenko, "Electromagnetic gyrokinetic pic simulation with an adjustable control variates method," *Journal of Computational Physics*, vol. 225, no. 1, pp. 568–590, 2007.

[54] R. Hatzky, T. M. Tran, A. Könies, R. Kleiber, and S. J. Allfrey, "Energy conservation in a nonlinear gyrokinetic particle-in-cell code for ion-temperature-gradient-driven modes in θ-pinch geometry," *Physics of Plasmas*, vol. 9, no. 3, pp. 898–912, 2002.

[55] S. J. Allfrey and R. Hatzky, "A revised δf algorithm for nonlinear pic simulation," *Computer physics communications*, vol. 154, no. 2, pp. 98–104, 2003.

[56] Y. Todo, "Properties of energetic-particle continuum modes destabilized by energetic ions with beam-like velocity distributions," *Physics of Plasmas*, vol. 13, no. 8, p. 082 503, 2006. DOI: 10.1063/1.2234296.

[57] Y. Todo, M. A. Van Zeeland, A. Bierwage, and W. Heidbrink, "Multi-phase simulation of fast ion profile flattening due to alfvén eigenmodes in a diii-d experiment," *Nuclear Fusion*, vol. 54, no. 10, p. 104 012, 2014. DOI: 10.1088/0029-5515/54/10/104012.

[58] Y. Todo, M. A. Van Zeeland, A. Bierwage, W. Heidbrink, and M. Austin, "Validation of comprehensive magnetohydrodynamic hybrid simulations for alfvń eigenmode induced energetic particle transport in diii-d plasmas," *Nuclear Fusion*, vol. 55, no. 7, p. 073 020, 2015. DOI: 10.1088/0029-5515/55/7/073020.

[59] G. W. Hammett and F. W. Perkins, "Fluid moment models for landau damping with application to the ion-temperature-gradient instability," *Physical review letters*, vol. 64, no. 25, p. 3019, 1990.

[60] D. Spong, B. Carreras, and C. Hedrick, "Nonlinear evolution of the toroidal alfvén instability using a gyrofluid model," *Physics of plasmas*, vol. 1, no. 5, pp. 1503–1510, 1994.

[61] J. Varela, D. Spong, and L. Garcia, "Analysis of alfven eigenmodes destabilization by energetic particles in tj-ii using a landau-closure model," *Nuclear Fusion*, vol. 57, no. 12, p. 126 019, 2017.

[62] D. A. Spong, "Long-term landau-fluid simulation of alfvén eigenmode instabilities," *Plasma and Fusion Research*, vol. 9, pp. 3 403 077–3 403 077, 2014.

[63] A. H. Boozer, "Establishment of magnetic coordinates for a given magnetic field," Princeton Univ., NJ (USA). Plasma Physics Lab., Tech. Rep., 1981.

[64] D. A. Spong, "Simulation of alfvén frequency cascade modes in reversed shear-discharges using a landau-closure model," *Nuclear Fusion*, vol. 53, no. 5, p. 053 008, 2013.

[65] C. Hedrick, J.-N. Leboeuf, and D. Spong, "Alpha-alfvén local dispersion relation and solutions," *Physics of Fluids B: Plasma Physics*, vol. 4, no. 12, pp. 3869–3882, 1992.

[66] C. Z. Cheng, "Kinetic extensions of magnetohydrodynamics for axisymmetric toroidal plasmas," *Phys. Reports*, vol. 211, pp. 1–51, Jan. 1992.

[67] G. J. Kramer, R. Nazikian, B. Alper, M. de Baar, G.-Y. Fu, N. N. Gorelenkov, G. McKee, S. D. Pinches, T. L. Rhodes, S. E. Sharapov, W. M. Solomon, and M. A. Van Zeeland, "Interpretation of core localized Alfvén eigenmodes in diii-d and joing european torus reversed magnetic shear plasmas," *Phys. Plasmas*, vol. 13, May 2006.

[68] H. Berk, R. Mett, and D. Lindberg, "Arbitrary mode number boundary-layer theory for nonideal toroidal alfvén modes," *Physics of Fluids B: Plasma Physics*, vol. 5, no. 11, pp. 3969–3996, 1993.

[69] Z. Wang, Z. Lin, I. Holod, W. Heidbrink, B. Tobias, M. Van Zeeland, M. Austin, *et al.*, "Radial localization of toroidicity-induced alfvén eigenmodes," *Physical review letters*, vol. 111, no. 14, p. 145 003, 2013.

[70] F. Zonca, L. Chen, and R. A. Santoro, "Kinetic theory of low-frequency alfvén modes in tokamaks," *Plasma physics and controlled fusion*, vol. 38, no. 11, p. 2011, 1996.

[71] M. Austin and J. Lohr, "Electron cyclotron emission radiometer upgrade on the diii-d tokamak," *Review of scientific instruments*, vol. 74, no. 3, pp. 1457–1459, 2003.